Journal of Building Performance Simulation

ISSN: 1940-1493 (Print) 1940-1507 (Online) Journal homepage: www.tandfonline.com/journals/tbps20

A user-friendly boiler model for dynamic simulations

Moritz Zuschlag, David Jansen, Rita Streblow & Dirk Müller

To cite this article: Moritz Zuschlag, David Jansen, Rita Streblow & Dirk Müller (16 Oct 2025): A user-friendly boiler model for dynamic simulations, Journal of Building Performance Simulation, DOI: 10.1080/19401493.2025.2572693

To link to this article: https://doi.org/10.1080/19401493.2025.2572693

JOURNAL OF BUILDING PERFORMANCE SIMULATION
https://doi.org/10.1080/19401493.2025.2572693

A user-friendly boiler model for dynamic simulations

Moritz Zuschlag, David Jansen, Rita Streblow and Dirk Müller

Institute for Energy Efficient Buildings and Indoor Climate, E.ON Energy Research Center, RWTH Aachen University, Aachen, Germany

ABSTRACT

Boilers are essential in energy systems, serving as primary heat suppliers, peak load units, backups, or high-temperature sources. Dynamic simulation helps to analyze their future roles and control strategies. Various modelling approaches exist. Reducing user-effort, a model should combine off-design operation, scalability, and user-friendly parameterization. This paper focuses on these aspects. First, it defines model requirements and reviews literature for compliance. Then, a new quasi-static simplified physical model is introduced, using 1-D heat transfer to calculate efficiency describing boiler operation in general. The general operation is described in a characteristic chart that maps efficiency to four operating conditions. The model is validated with field- and manufacturer data. Finally, the efficiency chart is tested in a Modelica implementation and compared with other efficiency estimation models. As the dynamic model is able to describe boiler operation in general, it requires minimal boiler-specific knowledge, ensuring easy parameterization, off-design operation, and scalability.

ARTICLE HISTORY
Received 5 May 2025
Accepted 30 September 2025

KEYWORDS
Boiler model; user-friendly; scalability; modular model; off-design; dynamic

1. Introduction

The heating sector is a large part of the German energy sector (Becker et al. 2022). The integration of renewable energies is of great interest to German policymakers as they seek to reduce the use of fossil fuels as part of the German energy transition. To integrate renewable energies, energy systems are becoming more complex in terms of their design and control (Bloess, Schill, and Zerrahn 2018; Verzijlbergh et al. 2017). Therefore, heat generators and their integration into building energy systems (BES) are of great importance in this respect. In German buildings, most of the installed and newly installed heat generators are natural gas boilers (Becker et al. 2022). However, due to an ongoing increase in heat pump systems (Bundesverband Wärmepumpe e.V., Branchenstudie 2023), boiler operating will become less dominant for space heating in the future. Two possible scenarios for future boiler operation are peak load operation and backup heating (Zeyen, Hagenmeyer, and Brown 2021). Apart from fossil operation, the manufacturers Viessmann (Viessmann Climate Solutions SE 2022) and Bosch (Kaletsch 2020) will offer boilers that can use green hydrogen. Other usable fuels for heating are biogas (International Energy Agency IEA 2020) or different kinds of wood (Becker et al. 2022). So, there are many possible scenarios to use boilers in the future.

To design complex BES, simulations (Attia et al. 2012; Loonen, De Klijn-Chevalerias, and Hensen 2019) and optimization (Andrew Bollinger, Marquant, and Sulzer 2019; Wirtz, Remmen, and Müller 2021) analyses can be carried out. Dynamic simulations are employed to provide a more realistic representation of system behaviour in comparison to optimization approaches (Maier et al. 2023). In order to conduct dynamic simulations of BES, dynamic models are needed to represent the slow-moving temperature process through the use of physics described by differential equations (Afram and Janabi-Sharifi 2014). In contrast, static models can be used to describe fast dynamics (Afram and Janabi-Sharifi 2014). To reduce the complexity of a model, grey-box models employ a combination of data-driven correlations and physical descriptions (Afram and Janabi-Sharifi 2014). In the modelling language Modelica, various libraries for building performance simulation are available (Maier et al. 2023; Senkel et al. 2021; Wetter et al. 2014). However, common Modelica grey-box boiler models typically require efficiency parameter data that must be obtained and implemented by the user (Maier et al. 2023; Senkel et al. 2021; Wetter et al. 2014), which reduces user-friendliness. Additionally, the ability to simulate complex off-design conditions highly depends on the quality and quantity of the efficiency parameter data. In particular the representation

CONTACT Moritz Zuschlag moritz.zuschlag@eonerc.rwth-aachen.de RWTH Aachen University, Mathieustrasse 10, 52074 Aachen, Germany

of condensation phenomena is challenging (Glembin et al. 2013; Simic et al. 2021). These issues can present significant barriers for practical application and limits model usability (Glembin et al. 2013; Gopisetty, Treffinger, and Xu 2014; Simic et al. 2021).

Gopisetty, Treffinger, and Xu (2014) highlight the need for 'generic simple boiler models' for energy planning. Such a model features easy parameterization, sizing by parameter variation, representation of start-up/shut-down and storage effects, and the use of predefined fluid properties (Gopisetty, Treffinger, and Xu 2014).

To address these challenges, this paper introduces a boiler model that combines user-friendly parameterization, scalability which addresses sizing by parameters, and off-design simulation capability. The goal is to minimize user effort by reducing dependence on manufacturer-specific data parameters, while maintaining sufficient accuracy for any possible design operating point and off-design operation, both with and without condensation effects. The research gap is discussed in more detail in Section 1.2.

In order to present a user-friendly boiler model, in the first part, this paper introduces a quasi-static simplified physical model (SPM) that describes the efficiency of a natural gas boiler's general operation, including condensation effects. The SPM is calibrated using multiple public available manufacturer exhaust temperature data that represent nominal operating conditions for a wide range of nominal boiler sizes to address scalability. Based on this calibration, the SPM can estimate various off-design efficiencies resulting in a general boiler operating estimation. This general operation is validated using two independent data sources. As many grey-box boiler models base on manufacturer efficiency data (Maier et al. 2023; Senkel et al. 2021; Wetter et al. 2014), detailed manufacturer efficiency data is used for validation mainly. In addition, a validation against efficiency data based on field monitoring data is presented.

In the second part, dynamic modelling and simulation is addressed. The quasi-static SPM is integrated into a dynamic, modular boiler model that aims to be representative of general natural gas boiler operation. Its parameterization is based solely on three parameters: design thermal power, and design supply and return temperatures. In conclusion, the novelty of this paper lies in the combination of both the SPM and the dynamic model, ensuring user-friendliness – since no detailed information needs to be provided by the user – while still enabling scalability and off-design operation.

1.1. State of the art boiler models

This subsection presents an overview about different boiler modelling approaches in terms of BES-simulation.

Simic et al. (2021) present a comprehensive literature review addressing boiler modelling. Their review demonstrated that the models are not applicable to diverse boiler types, sizes, and operational conditions. In addition, they point out a need for minimal calibration effort.

To address this gap, Simic et al. (2021) present a comprehensive modelling approach to heat exchange, based on thermodynamic laws, which places particular emphasis on the utilization of publicly available manufacturer information. In this approach, the boiler is separated into three parts combustion, heat transfer, and chimney. Inputs are taken from the publicly available manufacturer data. In the model, the envelop losses and a factor to describe the heat exchanger dew point effectiveness are fitted being parameters. The model can switch between condensing and non-condensing modes. A single part-load measurement is used for validation, which demonstrates good accuracy.

In regard to the work by Simic et al. (2021), the user must possess the publicly available data to parameterize the model. Additionally, the amount of condensate is needed for the parameter heat exchanger dew point effectiveness (Simic et al. 2021). The amount of condensate is not always given in publicly available data. In addition, the approach by Simic et al. (2021) yields a suited representation of a specific boiler operation, but the model does not enable scalability directly.

Yang et al. (2023) used the logarithmic mean temperature difference from Simic et al. (2021) to develop a model of a hydrogen-enriched natural gas-fired condensing boiler. In their work energy savings and thermal performance were investigated. The boiler efficiency increases in dependency on hydrogen-enrichment (Yang et al. 2023).

Mojica-Cabeza et al. (2021) present a review of various methodologies for calculating and modelling boiler efficiency. In their review, they differentiate among three methodologies: analytical, mechanistic, and empirical. They point out that all methods rely on data, necessitating the measurement of various operating variables.

In the context of their call for 'generic simple boiler models', Gopisetty, Treffinger, and Xu (2014) present a dynamic boiler model which can be easily parameterized. This model was developed in Modelica representing a counter-flow heat exchange. The temperature of both

the water and the exhaust is calculated using the thermal conductance to the wall of heat transfer. In their work, a real boiler was employed to calculate the area of heat transfer. Furthermore, they highlight the challenges associated with using a few parameters and the enabling of a dynamic model.

Like the work by Simic et al. (2021) and Gopisetty, Treffinger, and Xu (2014), Glembin et al. (2013) tackle parameterization effort. Glembin et al. (2013) have identified five types of parameterization challenging a combination of easy parameterization and high accuracy. On this basis, they present a boiler model to fulfil both, easy parameterization and high accuracy, in terms of BES simulation. It is divided into a stationary and a dynamic modelling part. The heat exchange is described by the NTU-efficiency method. The dynamic part describes both, the flue gas and the water side. For parameterization without condensation, values are obtained from publicly available data. To describe the influence of condensation, their model needs additional measurements of the moisture. They point out that manufacturers do not publish this data usually. In conclusion, apart from condensation and dynamic operation, their model can be parameterized by one measurement of full load efficiency. For condensation, measurement of moisture for different power levels is required.

Another model in the context of space heating simulation is presented by Haller et al. (2011a). They present a semi-physical model that is divided into the parts combustion chamber, heat transfer, and thermal boiler output to describe the effects of space heating return temperature, power modulation, and condensation gains on the exhaust temperature. The heat transfer can be described by different modelling approaches (Haller et al. 2011a):

(1) The 'empirical delta-T approach' assumes a temperature difference between the water return flow and the exhaust flow. Measurements have shown a dependency on power modulation and water mass flow rate resulting in boiler-specific parameters that must be determined by experiments.
(2) The 'empirical effectiveness approach' uses the empirical heat exchanger effectiveness. It is assumed to be dependent on the base effectiveness at nominal conditions and correction terms for different operating conditions. Therefore the power modulation and the water mass flow rate are respected.
(3) The 'effectiveness-NTU approach' splits the heat exchanger into a section with and without condensation. A relationship for the effectiveness which depends on the heat exchanger coefficient of the section and the capacity streams of water and exhaust is described.

In a second work, Haller et al. (2011b) tested the three heat exchange models against measurements resulting in good accuracy. In the case of condensation, the 'effectiveness-NTU approach' presented the best accuracy but required more parameterization effort (Haller et al. 2011b). According to Simic et al. (2021) the presented approaches by Haller et al. (2011a) are difficult to apply because of experimental requirements.

In addition to the models presented so far, many boiler models have been published via Modelica open source BES-libraries (Maier et al. 2023; Senkel et al. 2021; Wetter et al. 2014).

The *Buildings* library (Wetter et al. 2014) presents the two boiler models `BoilerPolynomial` and `BoilerTable`. `BoilerPolynomial` uses user-selec table polynomial functions to determine the efficiency in dependency on the part load. The polynomials are of different orders. There are three variants: (1) the efficiency is constant for part load, (2) it is a function only of part load ratio, or (3) it depends on both part load and supply temperature. The constants of the polynomials represent the nominal efficiency and part load refers to the nominal fuel mass flow. `BoilerTable` bases on an efficiency chart that is used via Modelica-records to estimate the efficiency in dependency on the return temperature and the part load.

The *TransiEnt* library (Senkel et al. 2021) contains two boiler models. The model `SimpleBoiler` uses a constant efficiency. The model `SmallGasBoiler` includes both static and dynamic options that utilize characteristic curves from manufacturer data to determine efficiency based on two aspects. The first aspect pertains to part load and describes the relative heating power, while the second aspect pertains to the return temperature.

The *AixLib* library (Maier et al. 2023) consists of the models `Boiler` and `BoilerNoControl`. Both use manufacturer data describing the efficiency as a function of the part load. The part load addresses the fuel mass flow. Furthermore, the model `BoilerNoControl` demonstrates the impact of return temperature on efficiency by employing a factor derived from a regression.

1.2. Research gap

As described above, parameterization is a major challenge in terms of boiler modelling. The previously described boiler models need different types of parameters based on the modelling approach. These parameters can be derived directly from measurements (Gopisetty, Treffinger, and Xu 2014; Haller et al. 2011a), or obtained from manufacturer data describing efficiencies (Maier et al. 2023; Senkel et al. 2021; Wetter et al. 2014). The provenance of public available manufacturer efficiency

data is often unclear or not explicitly documented. This may refer either to the origin of the values themselves (e.g. measurement or equation fit) or to unspecified operating conditions such as air–fuel ratio, water mass flow, or temperature difference. Next to this, as described for heat pumps, the use of manufacturer data can introduce uncertainties due to data variability (Olympios et al. 2020).

While it is possible to estimate the effort required to access values for parameterization (Blervaque et al. 2015), the parameterization of BES-models is a major challenge for modelling and simulation (Blervaque et al. 2015; Remmen et al. 2018; Wüllhorst et al. 2022, 2023). To tackle the implementation, in terms of BES, user-friendly templates for parameterization are a necessary feature for heating, ventilation and air conditioning (HVAC)-systems (Attia et al. 2012). As the previous analysis of Modelica models revealed, boiler behaviour is often described using a stationary efficiency chart (Maier et al. 2023; Senkel et al. 2021; Wetter et al. 2014). In those libraries, data sheets are cited as the source, so a dataset is treated as a parameter (Maier et al. 2023; Senkel et al. 2021; Wetter et al. 2014). One method of addressing parameterization effort is to supply parameter values (e.g. capacities and efficiency data) through a library, such as by utilizing Modelica records that correspond to the models for individual hardware configurations (Maier et al. 2023; Wüllhorst et al. 2023). For boilers, on the one hand, most public available manufacturer data sheets only provide efficiency data for two return temperatures (60°C and 30°C) and one (full-load) or two load points (additional part-load point) corresponding to these return temperatures. On the other hand, some data sheets provide efficiency charts of varying scope.

However, in the libraries (Maier et al. 2023; Senkel et al. 2021; Wetter et al. 2014) no discussion is presented on how to treat different data concerning amount, nominal power and operating conditions. Consequently, the user has to decide what efficiency parameterization data is suitable. This, combined with the implementation of values, reduces user-friendliness. Additionally, due to the small amount of operating conditions covert by manufacturer data a potential conflict that occurs is how to treat extrapolation. Extrapolation is quite challenging as it may result in errors (Brooks, Carroll, and Verdini 1988; Jin and Spitler 2002; Rätz et al. 2024; Wüllhorst et al. 2021).

All of the previously described topics may reduce the quality of simulation results and their comparability. In conclusion, the aforementioned factors can challenge the usability of a model and the feasibility of a parameter study, leading to the following questions regarding the use of efficiency data from manufacturer, which is limited by three key questions:

- Does the efficiency data represent nominal/design conditions correctly?
- Does the efficiency data represent off-design conditions correctly?
- Does the efficiency data variability under nominal/design conditions affect the simulation results?

As presented in Section 1.1, Gopisetty, Treffinger, and Xu (2014) introduces a call for a simple boiler model to support energy planning presenting four requirements: emphasizing easy parameterization, dimension by parameter variation, representation of start-up/shut-down and storage effects, and the use of predefined fluid properties. The three presented questions support their call for the use of user friendly boiler models in energy planning.

Simic et al. (2021) and Glembin et al. (2013) identify the modelling of condensation effects as a significant factor contributing to the increased effort required for parameterization. But the model by Gopisetty, Treffinger, and Xu (2014) does not respect condensation. In addition, their model uses two parameters of thermal conductance resulting in a significant challenge in terms of scalability as both parameters base on geometries.

Finally, to the best of the authors' knowledge, no existing boiler model satisfies the requirements identified by Gopisetty, Treffinger, and Xu (2014) – namely, easy parameterization and dimension by parameter variation which is addressed by scalability. Thus, the literature lacks models that combine user-friendliness – through easy parameterization and scalability – with the capability to simulate complex off-design behaviour, including condensation effects. In summary, a model is needed that balances the trade-off between parameterization effort and overall model fidelity representing natural gas boiler operation in general.

2. Simplified physical boiler model

This section introduces the quasi-static SPM representing a boiler model. The main task of a boiler is to deliver a heat flow to a heating system. For this purpose, Figure 1 presents a simplified boiler with its inner heat exchanger. The return water flow (T_{return}) enters the heat exchanger on the cold side, while the cold exhaust (T''_{ex}) leaves it. On the hot side, the hot exhaust enters (T'_{ex}) and the supply water flow (T_{supply}) exits. The burner and the fuel supply are located at the bottom.

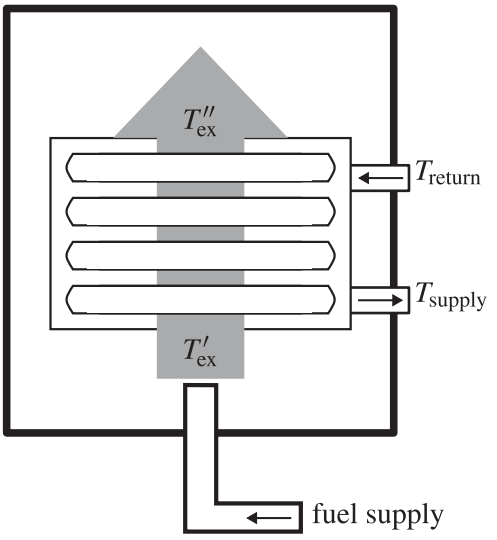

Figure 1. Simplified boiler design.

Generally, an operating point for a transferred heat flow $\dot{Q}_b$ can be described in dependency on the water mass flow $\dot{m}_w$, T_{return}, and T_{supply}. For design (des) conditions, they are used in Equation (1).

$$\dot{Q}_b^{des} = \dot{m}_w^{des} \cdot c_{p,w} \cdot (T_{supply}^{des} - T_{return}^{des}) \quad (1)$$

The relative thermal boiler power y_b is characterized by off-design conditions. The reference for y_b is the design thermal boiler power $\dot{Q}_b^{des}$. As defined by Equation (2), the thermal power can be partitioned into two components: the relative thermal power derived from the water mass flow control, represented by y_w, and the relative thermal power derived from the supply temperature control, represented by $y_{\Delta T}$.

$$y_b = \frac{\dot{Q}_b}{\dot{Q}_b^{des}} = \frac{\dot{m}_w}{\dot{m}_w^{des}} \cdot \frac{T_{supply} - T_{return}}{T_{supply}^{des} - T_{return}^{des}} = y_w \cdot y_{\Delta T} \quad (2)$$

The design and off-design perspectives completely characterize the heat allocation. The boiler's characteristics must be described based on the four presented dimensions $f(T_{return}, T_{supply}, y_w, y_{\Delta T})$.

The firing rate is equivalent to the relative fuel mass flow y_{fuel}. Equation (3) presents y_{fuel} which is referenced on the design fuel mass flow $\dot{m}_{fuel}^{des}$. The combustion power $\dot{Q}_{fuel}^{HHV}$ is based on the higher heating value *HHV*.

$$y_{fuel} = \frac{\dot{Q}_{fuel}^{HHV}}{\dot{Q}_{fuel}^{HHV,des}} = \frac{\dot{m}_{fuel} \cdot HHV}{\dot{m}_{fuel}^{des} \cdot HHV} \quad (3)$$

Equation (4) describes the energy balance. The thermal boiler power $\dot{Q}_b$ presents the usable heat flow. The losses consist of the exhaust enthalpy flow $\dot{H}_{ex}$ and the heat flow to the ambient $\dot{Q}_{amb}$. The moment when condensation occurs depends on the condensation temperature T_{cond}. In this situation, an additional enthalpy flow of the condensate $\dot{H}_w$ appears.

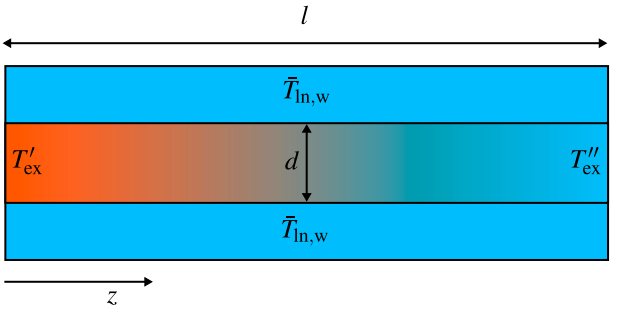

Figure 2. Simplified heat exchanger design.

$$\dot{Q}_{fuel}^{HHV} = \begin{cases} \dot{Q}_b + \dot{Q}_{amb} + \dot{H}_{ex} & T''_{ex} > T_{cond} \\ \dot{Q}_b + \dot{Q}_{amb} + \dot{H}_{ex} + \dot{H}_w & T''_{ex} \leq T_{cond} \end{cases} \quad (4)$$

In this work, heat transfer is the primary focus, while combustion is assumed to be ideal. The SPM combines mathematical correlations and physical equations to describe heat transfer. This SPM models the boiler but depends only on the four presented dimensions. It calculates efficiency for different quasi-static operating points. As stated in Simic et al. (2021), this work only utilizes data from publicly available manufacturer documentation.

2.1. Exhaust temperature model

It is assumed that the heat exchanger operates in counterflow mode. The temperature profile of the water flow along the heat exchanger is unknown. Figure 2 illustrates the following assumption of this simplified heat exchanger. The temperature difference between return and supply is assumed to be small compared to the difference between T'_{ex} and T''_{ex}. Therefore, a constant mean water temperature is assumed, represented by the logarithmic mean temperature $\bar{T}_{ln,w}$. The heat exchanger is represented as a pipe with a length l and an inner diameter d. The exhaust stream is in the centre. It is surrounded by water with the constant temperature $\bar{T}_{ln,w}$.

The differential equation (5) simplifies the heat exchange in a pipe under the assumption of one-dimensional, steady-state heat transfer through a cylindrical wall, approximated as a flat surface. It is based on the conservation of energy and relates the axial enthalpy gradient $\frac{\partial \dot{H}_{ex}}{\partial z}$ of the exhaust gas to the local temperature difference between the exhaust gas and the wall. The heat transfer coefficient k characterizes the heat transfer from exhaust gas to water. The specific heat capacity $c_{p,ex}$ is

assumed to be constant and representative of the temperature range. The exhaust gas mass flow $\dot{m}_{ex}$ is moist and forms the sum of the air- and fuel mass flow.

$$\frac{\partial \dot{H}_{ex}}{\partial z} = \dot{m}_{ex} \cdot c_{p,ex} \cdot \frac{\partial T_{ex}}{\partial z} = -k \cdot \pi d \cdot (T_{ex} - \bar{T}_{ln,w}) \quad (5)$$

$$\int_{T'_{ex}}^{T''_{ex}} \frac{1}{(T_{ex} - \bar{T}_{ln,w})} \partial T_{ex} = \int_0^l \frac{-k \cdot \pi d}{\dot{m}_{ex} \cdot c_{p,ex}} \partial z \quad (6)$$

Concerning (Haller et al. 2011a; Simic et al. 2021) the heat exchanger coefficient kA_{hex} is identified to be a suitable physical property. Equation (7) describes kA_{hex}. The surface of the heat exchanger A equals a pipe layer. In Equation (8), T''_{ex} is described as a combination of Equation (6) and (7). As presented by Gopisetty, Treffinger, and Xu (2014), the adiabatic flame temperature can be assumed to be linearly correlated with the combustion-air ratio λ. To simplify, T'_{ex} is equivalent to the adiabatic flame temperature. A constant $\lambda = 1.155$ is used. The basis for this is the information 10 % CO_2 (Viessmann Werke GmbH & Co. KG 2017a, 2017b, 2018a, 2019a, 2019b) in dry exhaust (DIN Deutsches Institut für Normung e. V. 2022).

$$kA_{hex} = k \cdot \pi d \cdot l \quad (7)$$

$$T''_{ex} = \bar{T}_{ln,W} + (T'_{ex} - \bar{T}_{ln,w}) \cdot \exp\left(-\frac{kA_{hex}}{\dot{m}_{ex} \cdot c_{p,ex}}\right) \quad (8)$$

For determination of T''_{ex} both, kA_{hex} and $\dot{m}_{ex}$ are unknown. Manufacturer data contain values of $\dot{Q}_b^{des}$ and T''_{ex} for the design conditions $T_{supply} = 80°C$ and $T_{return} = 60°C$. Thus, all values necessary for calculating the logarithmic mean temperature difference *LMTD* (Equation (9)) are known. Manufacturers present similar values for T''_{ex}. Therefore, according to Equation (10), kA_{hex} can be assumed to be proportional to $\dot{Q}_b^{des}$, as described in Equation (11). The gradient $\frac{\partial kA_{hex}}{\partial \dot{Q}_b^{des}}$ is determined in the calibration which is presented in Section 2.3. For further modelling, $\frac{dkA_{hex}}{d\dot{Q}_b^{des}}$ is assumed to be constant for all operating points.

$$LMTD = \frac{T''_{ex} - T_{supply} - (T'_{ex} - T_{return})}{ln\left(\frac{T''_{ex} - T_{supply}}{T'_{ex} - T_{return}}\right)} \quad (9)$$

$$kA_{hex} = \frac{\dot{Q}_b^{des}}{LMTD} \quad (10)$$

$$kA_{hex} = \frac{\partial kA_{hex}}{\partial \dot{Q}_b^{des}} \cdot \dot{Q}_b^{des} \quad (11)$$

In the model, a simplified combustion of methane is assumed. Equation (12) describes the gross reaction equation in dependency on λ.

$$CH_4 + 2\lambda O_2 + 2\lambda \tfrac{79}{21} N_2 \rightarrow CO_2 + 2H_2O + 2(\lambda - 1)O_2 + 2\lambda \tfrac{79}{21} N_2 \quad (12)$$

Equation (12) is used on the one hand to determine the air requirement L_λ and on the other hand to determine the relative dry exhaust mass flow w_λ^{dry} which is based on the fuel mass flow. Both are given as a function of λ.

$$L_\lambda = \frac{2\lambda M_{O_2} + 2\lambda \frac{79}{21} M_{N_2}}{M_{CH_4}} \quad (13)$$

$$w_\lambda^{dry} = \frac{M_{CO_2} + 2\lambda \frac{79}{21} M_{N_2} + 2(\lambda - 1) M_{O_2}}{M_{CH_4}} \quad (14)$$

In the model, $\dot{Q}_{amb}$ is unknown. Therefore, an adiabatic boiler is the first to be considered. The adiabatic exhaust mass flow $\dot{m}_{ex}^{ad}$ can be determined based on the adiabatic fuel mass flow $\dot{m}_{fuel}^{ad}$ and the absolute humidity of the intake air x_{air} in Equation (15).

$$\dot{m}_{ex}^{ad} = \dot{m}_{fuel}^{ad} \cdot (L_\lambda \cdot (1 + x_{air}) + 1) \quad (15)$$

In case of an adiabatic boiler, $\dot{m}_{fuel}^{ad}$ depends on the adiabatic boiler efficiency η_b^{ad}, $\dot{Q}_b$ and the *HHV*.

$$\dot{m}_{fuel}^{ad} = \frac{\dot{Q}_b}{\eta_b^{ad} \cdot HHV} \quad (16)$$

Therefore, it is assumed that there is a possible alternative expression for the exponent from Equation (8). In Equation (17), this exponent can be estimated with the use of the Equations (11), (15) and (16). The exponent is called α.

$$\frac{kA_{hex}}{\dot{m}_{ex}^{ad} \cdot c_{p,ex}} = \frac{\frac{\partial kA_{hex}}{\partial \dot{Q}_b^{des}} \cdot \dot{Q}_b^{des}}{\frac{\dot{Q}_b}{\eta_b^{ad} \cdot HHV} \cdot (L_\lambda \cdot (1 + x_{air}) + 1) \cdot c_{p,ex}} = \frac{\frac{\partial kA_{hex}}{\partial \dot{Q}_b^{des}} \cdot \eta_b^{ad} \cdot HHV}{y_b \cdot (L_\lambda \cdot (1 + x_{air}) + 1) \cdot c_{p,ex}} = \alpha \quad (17)$$

Finally, T''_{ex} can be calculated independently of $\dot{Q}_b^{des}$ in Equation (18).

$$T''_{ex} = \bar{T}_{ln,w} + (T'_{ex} - \bar{T}_{ln,w}) \cdot \exp(-\alpha) \quad (18)$$

For further calculations, T''_{ex} is assumed to be equal to a non-adiabatic boiler. Therefore, η_b^{ad} is used to describe $\dot{Q}_{amb}$, too.

$$\eta_b^{ad} = \frac{\dot{Q}_b}{\dot{m}_{fuel}^{ad} \cdot HHV} = \frac{\dot{Q}_b + \dot{Q}_{amb}}{\dot{m}_{fuel} \cdot HHV} \quad (19)$$

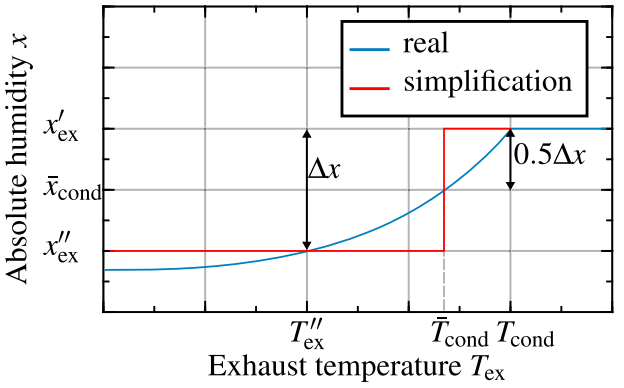

Figure 3. Simplification of the condensation model against a real assumption for x.

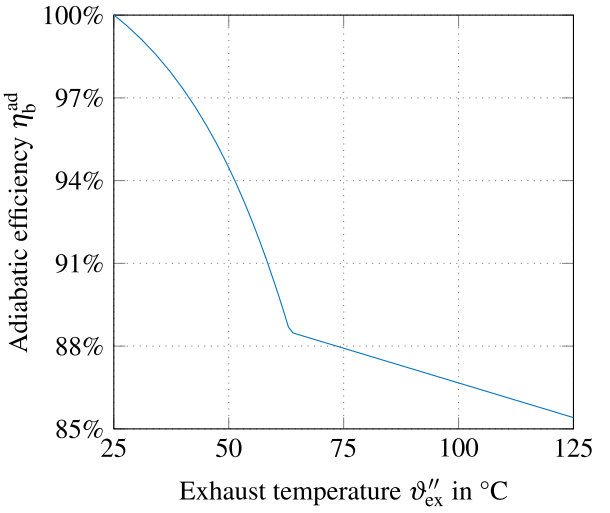

Figure 4. Calculated η_b^{ad} for an intake air temperature of 25°C and a relative humidity of 100%.

2.2. Efficiency model

In Equation (17), used in Equation (18), η_b^{ad} is unknown. For its prediction, condensation has to be respected if $T''_{ex} \leq T_{cond}$. If condensation occurs, an additional latent heat flow has to be added. Based on a simplified model of moisture distribution developed for this work Figure 3 introduces the corresponding assumptions and simplifications. The absolute humidity after combustion x'_{ex} is presented in Equation (20). It depends on a given absolute humidity of the intake air x_{air}.

$$x'_{ex} = \frac{x_{air} \cdot L_\lambda + 2 \cdot \frac{M_{H_2O}}{M_{CH_4}}}{w_\lambda^{dry}} \tag{20}$$

Assuming instantaneous condensation at $\bar{T}_{cond}$, rather than continuous condensation for $T_{ex} \leq T_{cond}$, x is represented in Equation (21). Equation 22 describes the amount of condensate Δx.

$$x(\bar{T}_{cond}) = x(T''_{ex}) + 0.5\Delta x = x(T'_{ex}) - 0.5\Delta x \tag{21}$$

$$\Delta x = x(T'_{ex}) - x(T''_{ex}) \tag{22}$$

Finally, based on a general energy balance of the exhaust gas, the transferred heat flow $\dot{Q}_b$ can be described without and with condensation in Equation (23).

$$\dot{Q}_b = \begin{cases} \dot{m}_{ex} \cdot c_{p,ex} \cdot (T'_{ex} - T''_{ex}) & T''_{ex} > T_{cond} \\ \dot{m}_{ex}^{dry} \cdot [c_{p,ex}^{dry} \cdot (\bar{T}_{cond} - T''_{ex}) \\ +\Delta x \cdot \Delta h_{vap} \\ +x''_{ex} \cdot c_{p,v} \cdot (\bar{T}_{cond} - T''_{ex}) \\ +(1 + x'_{ex}) \cdot c_{p,ex} \cdot (T'_{ex} - \bar{T}_{cond})] & T''_{ex} \leq T_{cond} \end{cases} \tag{23}$$

Thus, for a given λ and by respecting Equation (19), Equation (24) introduces η_b^{ad} only in dependency on T''_{ex} for both cases.

$$\eta_b^{ad} = \begin{cases} \frac{(L_\lambda \cdot (1 + x_{air}) \cdot c_{p,ex} \cdot (T'_{ex} - T''_{ex})}{HHV} & T''_{ex} > T_{cond} \\ w_\lambda^{dry} \frac{c_{p,ex}^{dry} \cdot (\bar{T}_{cond} - T''_{ex})}{HHV} \\ +w_\lambda^{dry} \frac{\Delta x \cdot \Delta h_{vap}}{HHV} \\ +w_\lambda^{dry} \frac{x''_{ex} \cdot c_{p,v} \cdot (\bar{T}_{cond} - T''_{ex})}{HHV} \\ +w_\lambda^{dry} \frac{(1 + x'_{ex}) \cdot c_{p,ex} \cdot (T'_{ex} - \bar{T}_{cond})}{HHV} & T''_{ex} \leq T_{cond} \end{cases} \tag{24}$$

An iterative approach is needed to solve Equation (18). As an example, Figure 4 presents η_b^{ad} in dependency on ϑ''_{ex} (°C) for an intake air temperature of 25°C and a relative humidity of 100%. As Figure 4 presents, for these inputs η_b^{ad} is 100% if the exhaust is equal to the intake air temperature.

2.3. Calibration

This section presents the calibration of the gradient $\frac{\partial kA_{hex}}{\partial \dot{Q}_b^{des}}$. In contrast to the approach taken by Simic et al. (2021), this work employs data exclusively from the temperature levels 80/60°C. As previously described, kA_{hex} is assumed to be proportional to $\dot{Q}_b^{des}$ and constant during operation under various off-design conditions. In the calibration process, kA_{hex} is estimated using a parameter sweep of $\frac{\partial kA_{hex}}{\partial \dot{Q}_b^{des}}$ in the SPM to calculate T''_{ex} (Equation (18)). For a first guess, Equation (10) can be used to give an overview of possible values based on the

manufacturer's temperature information. In the parameter sweep, the estimated values for kA_{hex} are valid if $|T''_{\mathrm{ex,SPM}} - T''_{\mathrm{ex,man}}| < 0.5$ K. From these values, the parameter value that results in the smallest error is selected for calibration.

Publicly available manufacturer data from 12 data sheets of three manufacturers (Max Weishaupt SE 2025; Viessmann Werke GmbH & Co. KG 2017c, 2018b, 2019a, 2019c, 2019d, 2020; Wolf GmbH 2009, 2015a, 2015b, 2015c, 2015d) are used to calibrate kA_{hex}. These data sheets present 45 boilers. Figure 5 shows the calibration. On the right y-axis, the histogram represents the data distribution as a function of $\dot{Q}_{\mathrm{b}}^{\mathrm{des}}$. As shown, the data is unevenly distributed with less data available for higher $\dot{Q}_{\mathrm{b}}^{\mathrm{des}}$. On the left y-axis, kA_{hex} is displayed. To address the unequal distribution, two calibrations are performed. From the entire dataset (black+gray markers), an evenly distributed subset (gray markers) is extracted. The extracted subset utilizes only the data point with the smallest error relative to mean value of each bin. This subset is highlighted in grey. For this data, a solid linear fit is applied. Additionally, a dotted linear fit represents the regression of the entire dataset (including the grey data). Both fits exhibit a high R^2 value and are close to each other. Consequently, the uneven data distribution does not significantly impact the calibration results. The fit is used to estimate $\frac{\partial kA_{\mathrm{hex}}}{\partial \dot{Q}_{\mathrm{b}}^{\mathrm{des}}}$ according to Equation (11). This feature enables the model to describe the efficiency independently of $\dot{Q}_{\mathrm{b}}^{\mathrm{des}}$ of the boiler, thereby facilitating its scalability.

Additionally, as used by Simic et al. (2021), this work employs a regression analysis for the heat exchanger coefficient of the housing kA_{housing}. It is used to simulate the heat flow through the housing, which represents the ambient losses $\dot{Q}_{\mathrm{amb}}$. In Equation (25) kA_{housing} is calculated. Standby losses are modelled according to P_{stby} from DIN EN 304 (DIN Deutsches Institut für Normung e. V. 2018). Some manufacturer data hold data about the coefficient q_{b}. It represents the heat losses as a percentage of the combustion power referred as the lower heating value *LHV* (DIN Deutsches Institut für Normung e. V. 2018). In this work, publicly available $q_{\mathrm{B,70}}$ data is used from two *V iessmann*-boilers: *VITOCROSSAL* 300 *Typ CM3C* (Viessmann Werke GmbH & Co. KG 2019a) and *VITOCROSSAL* 300 *Typ CR3B* (Viessmann Werke GmbH & Co. KG 2017c). It represents losses for a mean boiler temperature of 70°C (Diefenbach et al. 2002). Assuming an ambient temperature of 20°C (DIN Deutsches Institut für Normung e. V. 2022) results in a temperature difference of 50 K.

$$kA_{\mathrm{housing}} = \frac{P_{\mathrm{stby}}}{50\,\mathrm{K}} = \frac{1}{50\,\mathrm{K}} q_{\mathrm{B,70}} \cdot \dot{Q}_{\mathrm{fuel}}^{\mathrm{LHV}} \qquad (25)$$

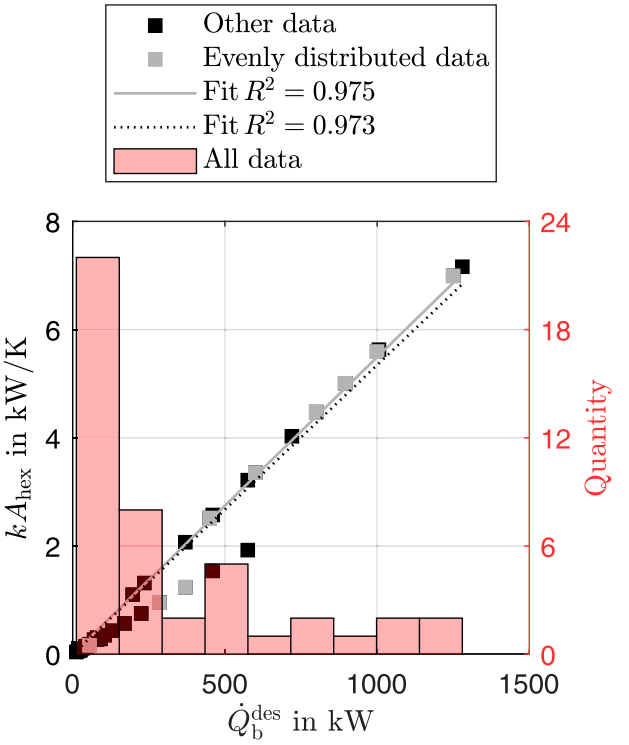

Figure 5. Data distribution and linear regression of kA_{hex} in dependency on $\dot{Q}_{\mathrm{b}}^{\mathrm{des}}$ for a supply temperature of 80°C and a return temperature of 60°C for 45 boilers.

To calculate kA_{housing}, a linear regression in dependency on $\dot{Q}_{\mathrm{b}}^{\mathrm{des}}$ is assumed. In Figure 6, this applies to calculated heat losses from the manufacturer's specifications mentioned above.

In summary, the fundamental aspects of this approach are that only publicly available data is used for modelling and calibration. This makes the approach independent of complex measurements and limits the number of possible parameters. In contrast to a measurement method, this approach therefore enables easy access to a large number of boilers. Furthermore, the calibration procedure can be applied to any other data set, either for individual boilers based on manufacturer data or for measurement data, with the purpose of designing a characteristic efficiency chart. For this reason, the presented assumptions and parameters may need to be re-evaluated and adjusted to ensure agreement with the respective operating conditions.

2.4. Validation

In this section, the SPM is compared with steady-state operating points. As stated previously, common grey-box boiler models are parameterized using efficiency charts derived from manufacturer data (Maier et al. 2023; Senkel et al. 2021; Wetter et al. 2014). Consequently, in

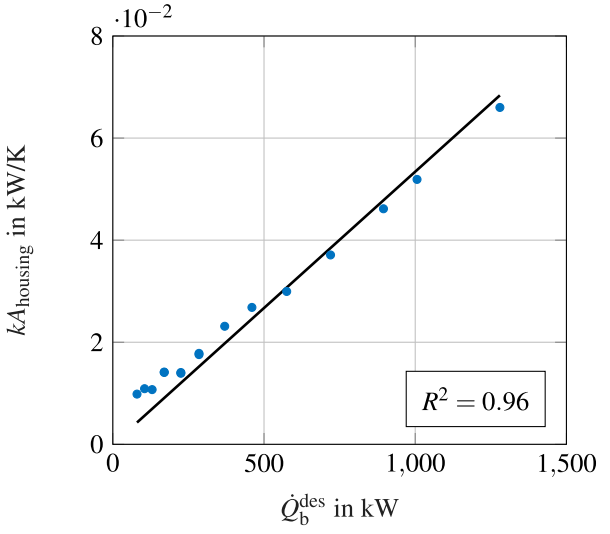

Figure 6. Linear regression of kA_{housing} in dependency on $\dot{Q}_{\text{b}}^{\text{des}}$ for a supply temperature of 80°C and a return temperature of 60°C.

this section the SPM is validated against detailed efficiency charts from manufacturer data. Furthermore, estimated efficiencies obtained from clustered time-series field-monitoring data of a real-world application are used to conduct a second validation.

2.4.1. Manufacturer efficiency data

In general, detailed efficiency data charts are hardly to obtain. But, some manufacturer provide detailed off-design information in addition to the limited number of data points under standardized conditions. For validation, efficiency charts for the boilers *V iessmann VITOCROSSAL* 200 *CIB* (Viessmann Werke GmbH & Co. KG 2019b) and *VITOCROSSAL* 300 *CRU* (800 kW-unit) (Viessmann Werke GmbH & Co. KG 2019e), describing η_{b} for different levels of supply/return-temperatures in dependency on the firing rate. In these data sheets, there is no information on how an efficiency chart was created – whether it is purely calculated or based on measurements with inter- and extrapolation. In addition, it is not clearly explained how the supply and return temperatures are adjusted during firing rate modulation. As no information is provided describing water mass flow control, in simulation, and for the manufacturer data, a supply-temperature-control is assumed to represent part-load resulting in $y_{\text{w}} = 1$. Additionally, both sheets (Viessmann Werke GmbH & Co. KG 2019b, 2019e) present T''_{ex}-data which is smaller than estimated $\bar{T}_{\text{ln,w}}$. So, according to Equation (18), both boilers cannot be part of the calibration.

The efficiency data of the *VITOCROSSAL* 200 *CIB* (Viessmann Werke GmbH & Co. KG 2019b) is based on the *LHV*.

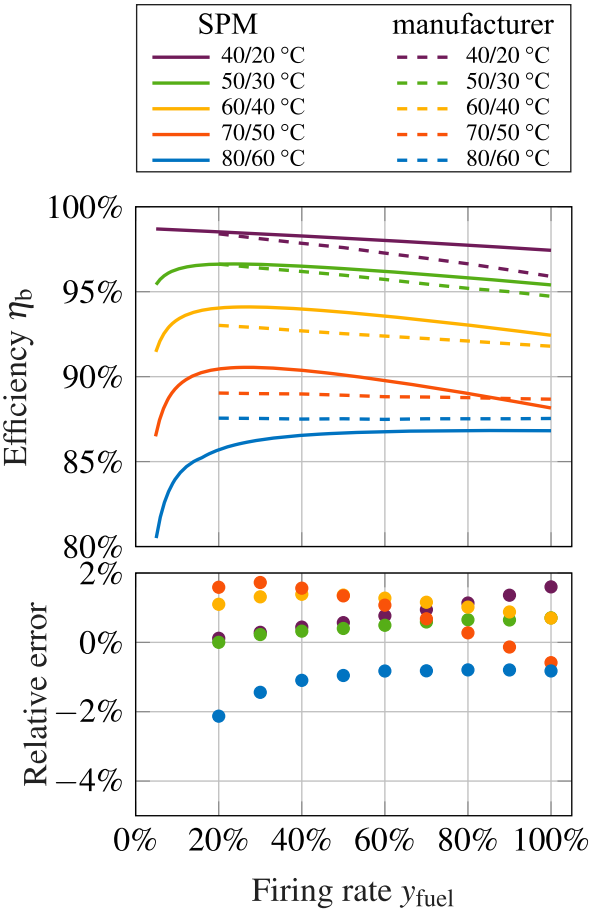

Figure 7. Validation with manufacturer data for *VITOCROSSAL* 200 *CIB* (Viessmann Werke GmbH & Co. KG 2019b). Manufacturer data are dashed and SPM results are solid. Color code represents supply/return-temperature in °C.

The SPM operates using the *HHV*, so for validation purposes, the efficiency data of the *VITOCROSSAL* 200 *CIB* (Viessmann Werke GmbH & Co. KG 2019b) is converted using $\frac{LHV}{HHV}$ for methane. Figure 7 presents, at the top, a comparison of the efficiency between SPM (solid) and converted manufacturer data (dashed). The colour code represents the supply/return-temperature region in °C. The data in Viessmann Werke GmbH & Co. KG (2019b) covers firing rates ranging from 20 % to 100 %. In general, the SPM accurately describes the effects of different design temperature levels on η_{b}. Additionally, it accounts for part-load phenomena by increasing η_{b} during part-load operation. The second plot presents the relative error, which overall lies between −2.13 % and 1.73 % of the corresponding efficiency of *VITOCROSSAL* 200 *CIB* (Viessmann Werke GmbH & Co. KG 2019b).

Figure 8 presents the SPM-validation and error analysis in comparison to the *V iessmann VITOCROSSAL* 300 *CRU* (800 kW-unit) (Viessmann Werke GmbH & Co. KG 2019e) for η_{b} at different levels of supply/return temperatures,

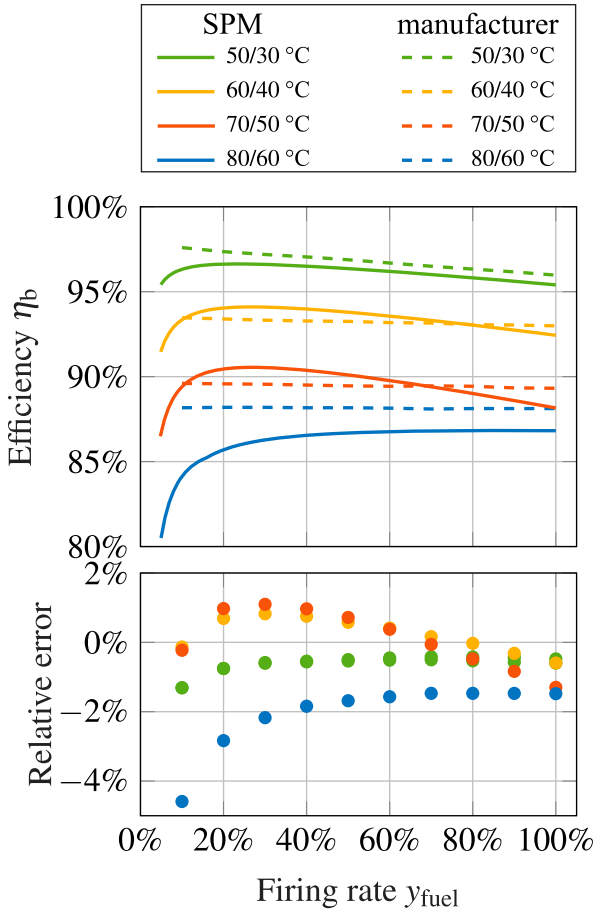

Figure 8. Validation with manufacturer data for *V ITOCROSSAL* 300 *Typ CRU* (800 kW-unit) Viessmann Werke GmbH & Co. KG (2019e). Manufacturer data are dashed and SPM results are solid. Color code represents supply/return-temperature in °C.

depending on the firing rate. Unlike the first boiler, the efficiency data of the *VITOCROSSAL* 300 *CRU* (Viessmann Werke GmbH & Co. KG 2019e) is based on *HHV* and provides additional data for $y_{fuel} = 10\%$, but not for the temperature region 40/20°C. As described previously, the SPM models both phenomena – temperature and part-load – well. The relative error lies between −4.59% and 1.10% of the corresponding efficiency of *VITOCROSSAL* 300 *CRU* (Viessmann Werke GmbH & Co. KG 2019e). The absolute error increases at low part-loads, especially at high temperatures.

In conclusion, the SPM is tested against two detailed manufacturer data sets. For both validations, the general operation described by the SPM accurately captures the efficiency across various operating conditions.

2.4.2. Field-monitoring data

This subsection compares the SPM with clustered time-series field-monitoring data. In comparison with manufacturer efficiency data, field-monitoring involves sensors for supply and return temperatures combined with fuel and water flow measurements, which clearly define the operating conditions. The field-monitoring data originates from the research project OOM4ABDO (Projektträger Jülich | Forschungszentrum Jülich GmbH 2017). In this project, the elco R3410 boiler with a nominal fuel power of 2 MW (ELCO GmbH 2013) is monitored. The monitoring cover data from January 16, 2023 to March 1 2024 with a 15 min resolution. In 2023, municipal utilities reported a *HHV*-range of 8.4 to 13.1 kWh/m^3 (SWM Infrastruktur GmbH und Co. KG 2024). For firing power calculation, the mean value of the *HHV*-range and the monitored gas flow rates (m^3/h) are used. Heating power is derived from water flow rates, supply-, and return temperatures. Efficiency is calculated at each operating point based on the fuel and heating power. In the first step of post-processing, data is filtered for steady-state operating points and measurement errors, reducing the dataset to 1858 data points. These are clustered by return temperature (±0.5 K) and firing rate (±2.5%). The largest clusters, representing 66% of the data, are considered. For comparison, the SPM is parameterized using a calculated nominal temperature spread of 26.52 K derived from field data. Further parameters, calculated from field data to describe operating conditions, are y_w, $y_{\Delta T}$, and the clustered T_{return}. Overall, 21 clusters are identified in dependency on T_{return} and firing rate.

Figure 9 illustrates the validation using the identified clusters. For comparison, the clusters are shown as a function of the corresponding y_b. The 21 clusters are displayed on the x-axis as $T_{return} \mid y_b$. The spread of T_{return} ranges from 44.6°C to 51.4°C, while y_b varies between 75.6% and 97.2%. In the first plot, the bars represent the identified field cluster efficiency η_b^{field}, with error bars indicating the standard deviation σ. Next to η_b^{field}, the estimated SPM efficiencies η_b^{SPM} are illustrated. In the second plot, the errors are shown: on the left, the difference between η_b^{field} and η_b^{SPM} is presented, while on the right, σ is displayed to provide context for the error magnitude. In conclusion, the errors are smaller than σ and remain within ±1.5%.

Next to the validation purpose, in the following a model comparison is presented. The data sheet provides efficiency data for two full-load temperature regimes (80/60°C: $\eta_b = 93.5\%$ and 40/30°C: $\eta_b = 94.5\%$) (ELCO GmbH 2013). Models as presented by Maier et al. (2023) and Wetter et al. (2014) or general steady investigations without further data would rely on these values. In comparison to efficiency values presented in Figure 9 these values deviate by approximately ±4%−−5% from both the SPM- and field data-based efficiencies. This discrepancy highlights the risk of relying on inappropriate manufacturer efficiency data, primarily due to the limited amount of available information. Consequently, the SPM

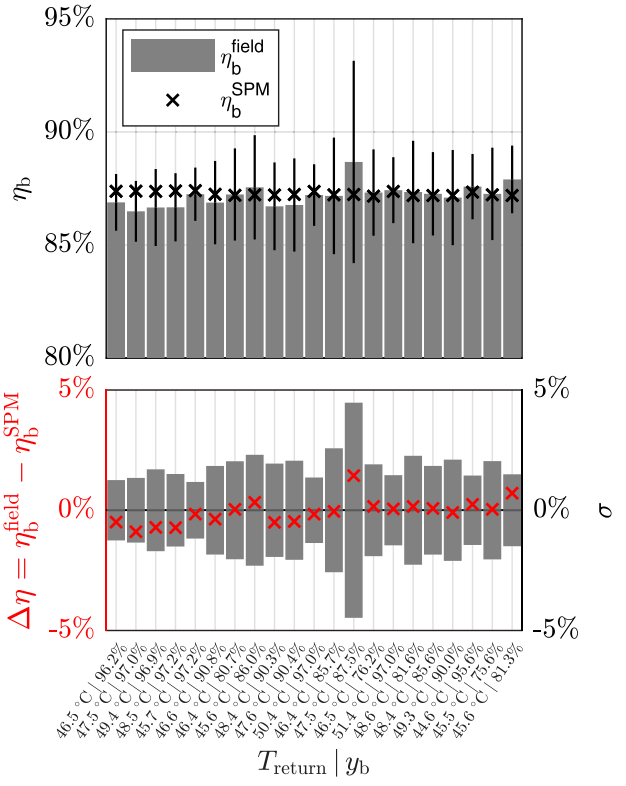

Figure 9. Validation with clustered field data in dependency on T_{return} and y_b; First plot presents efficiencies and belonging standard deviations σ of clustered field data. Second plot compares error $\Delta\eta$ with σ.

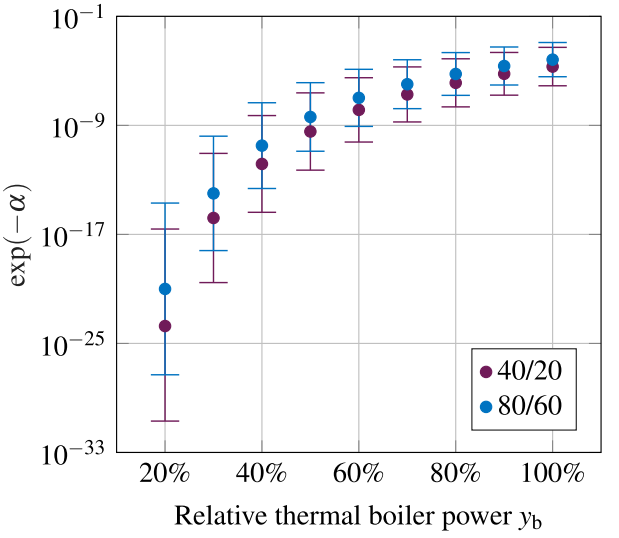

Figure 10. Sensitivity of the factor $\exp(-\alpha)$ used in Equation (18) to ±30% of $\frac{\partial kA_{hex}}{\partial \dot{Q}_b^{des}}$. Color code represents design supply/return-temperature in °C.

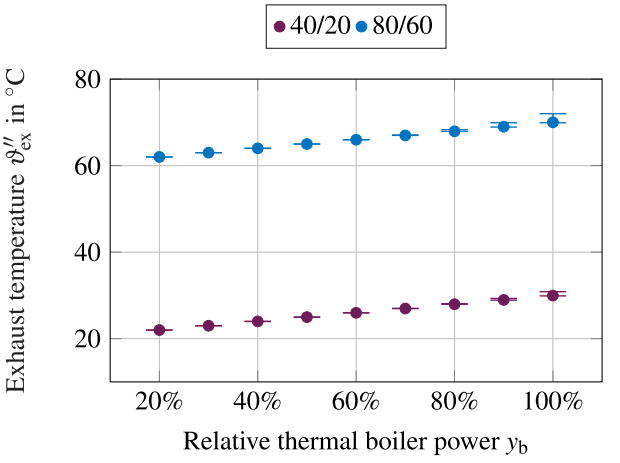

Figure 11. Sensitivity of the of the exhaust temperature ϑ''_{ex} to the factor $\exp(-\alpha)$ described in Figure 10. Color code represents design supply/return-temperature in °C.

is able to represent real steady-state operating conditions more accurately than the provided manufacturer efficiency data.

In conclusion, the SPM is tested against both field-monitoring and detailed manufacturer data. Overall, data is collected from three different boilers under various part-load conditions and temperature levels. For both validations, the general operation described by the SPM accurately captures the efficiency across various operating conditions. Therefore, assuming a constant kA_{hex} corresponding to the full-load operating point at 80/60°C can be regarded as a valid simplification. In addition, the validation confirms that the proposed parameter assumptions are suitable for describing boiler operation across a wide operating range.

2.5. Sensitivity

This subsection describes the sensitivity of the system to the gradient $\frac{\partial kA_{hex}}{\partial \dot{Q}_b^{des}}$ which is estimated within calibration. This gradient tackles the exhaust temperature calculation according to Equation (18). For sensitivity analysis ±30% of $\frac{\partial kA_{hex}}{\partial \dot{Q}_b^{des}}$ are used. Figure 10 illustrates the sensitivity of the resulting factor $\exp(-\alpha)$, as used in Equation (18), with respect to y_b. It is presented for a cold 40/20°C and a hot temperature region 80/60°C. For decreasing y_b, $\exp(-\alpha)$ and its variability are negligibly small.

Figure 11 illustrates the resulting sensitivity of the exhaust temperature ϑ''_{ex}, showing a maximum difference of 2 K under the 80/60°C full-load condition and a maximum difference of 0.91 K under the 40/20°C full-load condition.

Following the preceding part, Figure 12 shows the impact on efficiency. For the temperature region 80/60°C, the difference of 2.00 K results in a maximum efficiency drop of −0.10 %. In the colder temperature region 40/20°C, a maximum efficiency drop of −0.15%

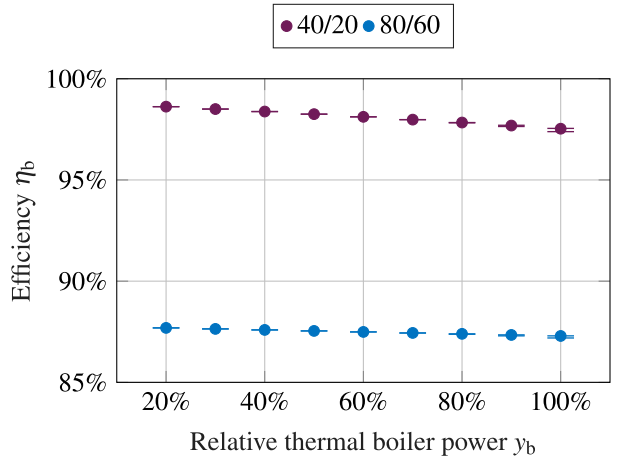

Figure 12. Sensitivity of the resulting efficiency representing the sensitivity of the system to the factor $\exp(-\alpha)$ described in Figure 10. Color code represents design supply/return-temperature in °C.

Table 1. Overview of operating conditions in the general characteristic chart.

Dependency	Min.	Max.	Step size
T_{return}	20°C	80°C	10 K
ΔT_{des}	2 K	30 K	2 K
y_w	5%	100%	5%
$y_{\Delta T}$	5%	100%	5%

is observed for a temperature difference of 0.91 K. Both values are within the error range, which was presented in Section 2.4.

3. Dynamic modular boiler model

This section introduces the new dynamic modular boiler model `BoilerModular`. It is part of the Modelica library *AixLib* (Maier et al. 2023). Figure 13 illustrates a simplified view of `BoilerModular`. It is divided into a dynamic model and a quasi-static model. As stated in Section 2.4, the calibrated SPM is capable of describing boiler operation in general. It is used to create a η_b^{ad}-chart that represents general boiler operation under various conditions. These are T_{return}, y_w, $y_{\Delta T}$ and the nominal temperature difference $\Delta T_{des} = T_{supply}^{des} - T_{return}^{des}$. Table 1 presents the various possible operating conditions represented by the dependencies in the general characteristic chart.

Further details of `BoilerModular` are presented below. `BoilerModular` is only parameterized by the three parameters $\dot{Q}_b^{des}$, T_{supply}^{des} and T_{return}^{des}. This convenient and user-friendly parameterization addresses a core element of the model by defining the design operating point.

The dynamic part of `BoilerModular` is based on the partial model `PartialHeatGenerator` which is

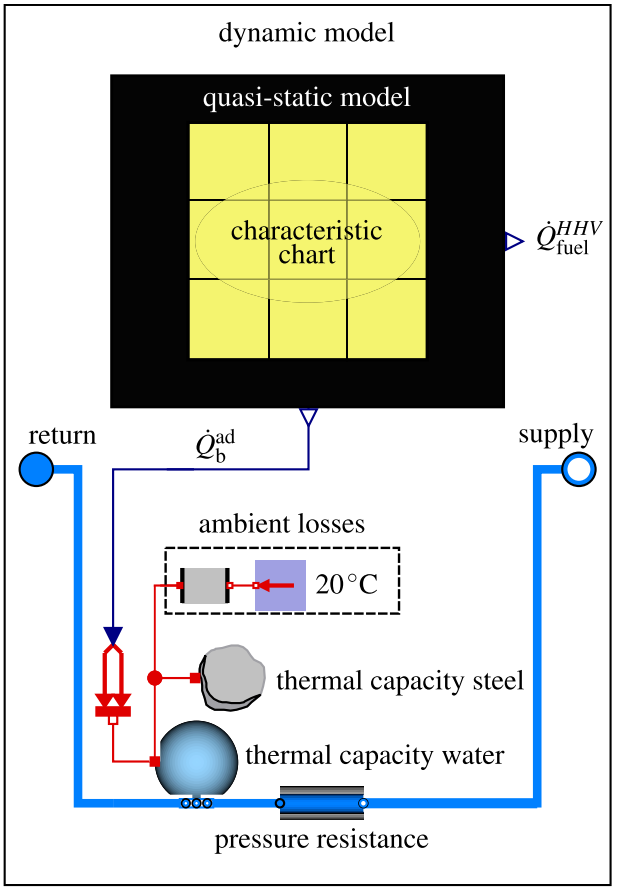

Figure 13. Simplified description of the dynamic model `BoilerModular`.

part of *AixLib* (Maier et al. 2023). To represent a thermal capacity `PartialHeatGenerator` consists of a water volume. In `BoilerModular`, this water volume is parameterized with a regression from manufacturer data in dependency on $\dot{Q}_b^{des}$. The model `BoilerNoControl` from *AixLib* (Maier et al. 2023) includes a second thermal capacity to account for the steel mass. This is in addition to the water volume. `BoilerModular` includes the steel mass and its parameterization. Additionally, `BoilerNoControl` (Maier et al. 2023) presents a thermal conductor to the ambient. This is also used in `BoilerModular`. The thermal conductor uses $kA_{housing}$. However, due to the 0-D modelling with a single volume, the difference between T_{amb} and T_{supply} is used instead of the mean boiler temperature, which leads to an overestimation of the losses. It is assumed that this is negligible. The heat flow $\dot{Q}_b^{ad}$ is transferred to the thermal capacities and the thermal conductor. The `PartialHeatGenerator` includes pressure resistance (Maier et al. 2023). It is parameterized based on manufacturer data through regression. `BoilerModular` can be connected to the heating system with the supply and return fluid ports.

The quasi-static model estimates the adiabatic heat flow $\dot{Q}_{\mathrm{b}}^{\mathrm{ad}}$ and the demand of fuel $\dot{Q}_{\mathrm{fuel}}^{\mathrm{HHV}}$. For `BoilerModular` it is assumed that the timescales of combustion and heat transfer are small compared to the timescales of these thermal capacities, resulting in a quasi-static representation. The quasi-static model is based on the SPM and the resulting chart is used in Modelica to reduce simulation time in comparison to an equation-based description. The chart is implemented via the scientific data format (SDF) which enables linear inter- and extrapolation in n-dimensional space in Modelica (Sommer, Andres, and Diehl 2014).

Figure 14 displays a schematic diagram that illustrates the basics of the quasi-static model. As presented previously, the operation can be divided into design and off-design. Thus, in the quasi-static model, this approach represents the two submodels, `DesignOperation` and `OffDesignOperation`. In both submodels, the 4D-$\eta_{\mathrm{b}}^{\mathrm{ad}}$-chart forms the core. As introduced, design operation is completely characterized by parameterization. Operating conditions define off-design operation. Further details on these submodels are listed below:

- `DesignOperation`:
  From parameterization $\dot{Q}_{\mathrm{b}}^{\mathrm{des}}$, $T_{\mathrm{supply}}^{\mathrm{des}}$ and $T_{\mathrm{return}}^{\mathrm{des}}$ are given. The design operating point is estimated in dependency on parameterization for full-load $\eta_{\mathrm{b}}^{\mathrm{ad,des}} = f(T_{\mathrm{supply}}^{\mathrm{des}}, T_{\mathrm{return}}^{\mathrm{des}}, 1, 1)$. The output $\eta_{\mathrm{b}}^{\mathrm{ad,des}}$ is therefore constant for the simulation. With it, this submodel characterizes the design operation by the design firing power $\dot{Q}_{\mathrm{fuel}}^{\mathrm{des}}$ using the design heat losses $\dot{Q}_{\mathrm{amb}}^{\mathrm{des}}$ additionally.

$$\dot{Q}_{\mathrm{amb}}^{\mathrm{des}} = kA_{\mathrm{housing}} \cdot (T_{\mathrm{supply}}^{\mathrm{des}} - T_{\mathrm{amb}}) \tag{26}$$

$$\dot{Q}_{\mathrm{fuel}}^{\mathrm{des}} = \frac{\dot{Q}_{\mathrm{b}}^{\mathrm{des}} + \dot{Q}_{\mathrm{amb}}^{\mathrm{HHV,des}}}{\eta_{\mathrm{b}}^{\mathrm{ad,des}}} \tag{27}$$

  This addresses a core element of the model by enabling scalability in terms of design thermal power and operating conditions.
- `OffDesignOperation`:
  The submodel `OffDesignOperation` represents the off-design operation. From `DesignOperation` $\dot{Q}_{\mathrm{fuel}}^{\mathrm{HHV,des}}$ is known and additionally the control variable y_{fuel} is given from the outside. Thus, the fuel power $\dot{Q}_{\mathrm{fuel}}^{\mathrm{HHV}}$ is known for each operating point.

$$\dot{Q}_{\mathrm{fuel}}^{\mathrm{HHV}} = y_{\mathrm{fuel}} \cdot \dot{Q}_{\mathrm{fuel}}^{\mathrm{HHV,des}} \tag{28}$$

  In addition to y_{fuel}, the off-design operating point is completely determined by T_{supply}, T_{return} and $\dot{m}_{\mathrm{w}}$. To get the inputs for the characteristic chart, the two relative variables $y_{\Delta\mathrm{T}}$ and y_{w} can be determined based on parameterization.

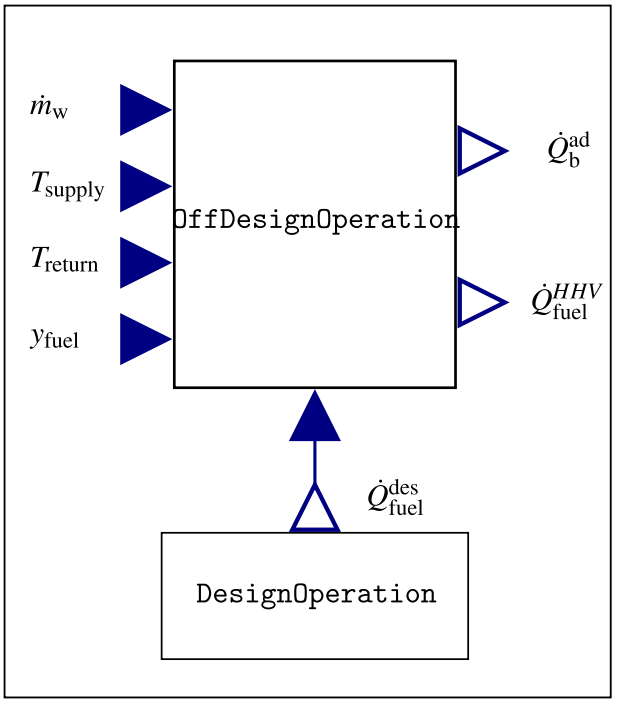

Figure 14. Simplified description of the quasi-static model. It combines the two submodels `OffDesignOperation` and `DesignOperation`.

$$y_{\Delta\mathrm{T}} = \frac{T_{\mathrm{supply}} - T_{\mathrm{return}}}{T_{\mathrm{supply}}^{\mathrm{des}} - T_{\mathrm{return}}^{\mathrm{des}}} \tag{29}$$

$$y_{\mathrm{w}} = \frac{\dot{m}_{\mathrm{w}}}{\dot{m}_{\mathrm{w}}^{\mathrm{des}}} \tag{30}$$

`OffDesignOperation` uses the same characteristic chart as `DesignOperation`, but with off-design operating conditions serving as the inputs. Thus from the chart, $\eta_{\mathrm{b}}^{\mathrm{ad}}$ is known $\eta_{\mathrm{b}}^{\mathrm{ad}} = f(T_{\mathrm{supply}}, T_{\mathrm{return}}, y_{\mathrm{w}}, y_{\Delta\mathrm{T}})$. This enables the calculation of $\dot{Q}_{\mathrm{b}}^{\mathrm{ad}}$ for the given operating point.

$$\dot{Q}_{\mathrm{b}}^{\mathrm{ad}} = \dot{Q}_{\mathrm{fuel}}^{\mathrm{HHV}} \cdot \eta_{\mathrm{b}}^{\mathrm{ad}} \tag{31}$$

In conclusion, the model is capable of simulating complex general off-design operation. Off-design conditions are characterized by temperature and mass flow control. This capability is derived from the general efficiency chart.

Apart from using the representative efficiency chart, `BoilerModular` can use any other efficiency chart that agrees with the presented dimensions.

4. Model comparison

In this section, a simulation study is presented for comparison purposes, focusing on the quasi-static efficiency

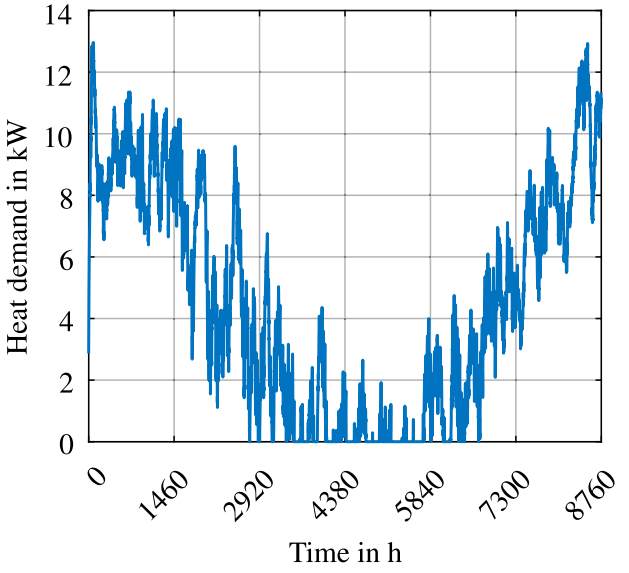

Figure 15. Simulated heat demand of a single family house.

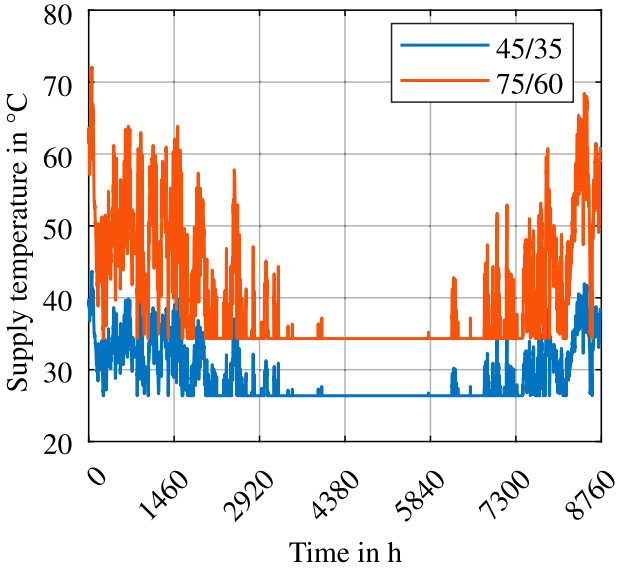

Figure 16. Supply temperature curves for the two design points 45/35°C and 75/60°C.

estimation method. As a test case a single-family house is used. Figure 15 illustrates the simulated heat demand of this house, based on a low-order building model (Schütz et al. 2017).

Additionally, the study is performed for the two design points 45/35°C and 75/60°C and belonging supply temperature control. In Figure 16, the corresponding supply temperature curves are shown based on the heating curve presented in *Buildings* library (Wetter et al. 2014).

The model developed in this work is compared with three efficiency estimation methods using data from boilers with different $\dot{Q}_{b}^{des}$. Table 2 presents an overview of different boilers with different $\dot{Q}_{b}^{des}$ from 12 to 800 kW. The amount of data is classified by evaluating the amount presented in the data sheet. As shown, it is difficult to obtain data for small boilers. To facilitate data comparison, it is necessary to adapt or assume the usability of some of the efficiency values, as detailed in the table caption. Therefore, for a first comparison, the efficiency is shown for the 80/60°C operating point. However, the efficiencies shown are quite similar. For comparison purposes, efficiency can be assumed to be independent of $\dot{Q}_{b}^{des}$.

Three quasi-static efficiency estimation methods, taken from *Aixlib* (Maier et al. 2023) and *Buildings* (Wetter et al. 2014) library, are used for comparison. The methods are used within the dynamic boiler model `BoilerNoControl` from *AixLib* (Maier et al. 2023). In the following, the three models are described in detail:

- *AixLib* (Maier et al. 2023):
  `BoilerNoControl` from *AixLib* library (Maier et al. 2023) is used which is parameterized with constant efficiency. During operation, the efficiency is corrected by the implemented data to respect the influence of the return temperature. For constant efficiency, the value from the WTC-GW data is used (Max Weishaupt GmbH 2023).
- 2D-table:
  `BoilerNoControl` (Maier et al. 2023) is modified to use 2D-table data instead. The efficiency is calculated with the use of bi-linear interpolation and extrapolation on the basis of the boiler data. The data depends on part-load and return temperature.
- Lin.-Quadratic:
  `BoilerNoControl` (Maier et al. 2023) is modified to use a linear-quadratic (lin.-quadratic) function instead. It is derived from the *Buildings* library (Wetter et al. 2014). The function includes a linear and quadratic term dependent on part-load and return temperature to describe efficiency. The coefficients are fitted based on the manufacture data.

All the proposed models necessitate individual boiler performance data, without any explicit physical description of the heat transfer mechanisms. The requisite data were obtained from publicly accessible boiler datasets Viessmann Werke GmbH & Co. KG (2019b, 2019e), and Lochinvar, LLC (2023b). These data were subsequently utilized to perform a linear-quadratic regression for η_{b}. As an alternative approach, the 2D-table representation of the data was parameterized using the given boiler datasets.

Figure 17 illustrates the corresponding annual fuel requirements for the three model approaches and the parameters of the four boilers for the design point

Table 2. boiler overview; efficiency for full-load return temperature 60°C: ∗ interpolated, ∗∗ transferred with *LHV*/*HHV* of methane, ∗∗∗ for 70°C mean boiler temperature.

Manufacturer	Boiler	$\dot{Q}_b^{des}$ in kW	Data amount	Efficiency	Reference
Weishaupt	WTC-GW	15–32	o	88.5%***	Max Weishaupt GmbH (2023)
Viessmann	200-W	12–150	–	88.7% **	Viessmann Werke GmbH & Co. KG (2018b)
Lochinvar	FTXL	117	++	87.9% *	Lochinvar, LLC (2024)
Lochinvar	Knight XL	117–293	++	87.4 *	Lochinvar, LLC (2023a)
Viessmann	CIB	80–636	+++	87.5 **	Viessmann Werke GmbH & Co. KG (2019b)
Lochinvar	FB-2501	703	++	87.8% *	Lochinvar, LLC (2023b)
Viessmann	CRU 800	800	++	88%	Viessmann Werke GmbH & Co. KG (2019e)

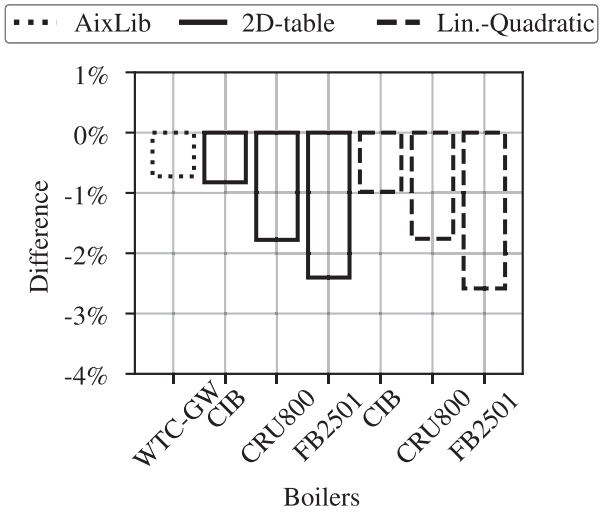

Figure 17. Difference in annual fuel demand for three efficiency estimation methods and four boilers in comparison to `BoilerModular` for the design point 75/60°C.

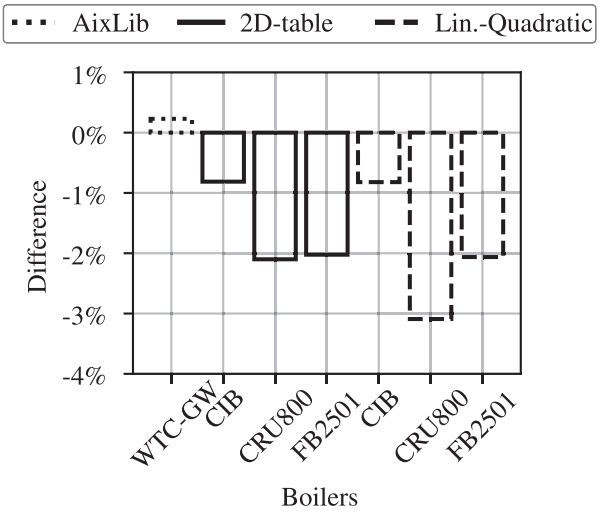

Figure 18. Difference in annual fuel demand for three efficiency estimation methods and four boilers in comparison to `BoilerModular` for the design point 45/35°C.

75/60°C. In comparison to `BoilerModular`, all model approaches underestimate the annual fuel demand by less than 3%. In both, the 2D-table and Linear-Quadratic, the lowest difference is achieved when simulating with parameters derived from CIB-data, as compared to CRU800- and FB2501-data. As listed in Table 2, the most data is available for the CIB-boiler. The manufacturer's data for FB2501 provides the least amount of data, and the results of the simulations are the most divergent for both the 2D-table and the linear-quadratic model.

Figure 18 illustrates the corresponding annual fuel requirements for the three model approaches and the parameters of the various boilers for the design point 45/35°C. In comparison to `BoilerModular`, only `BoilerNoControl` from *AixLib* overestimates the fuel demand by less than 1%. All other approaches underestimate the fuel demand by less than approx. 3%. Referring to the data amount, the CRU800-data (Viessmann Werke GmbH & Co. KG 2019e) do not agree with all operating conditions given in Figure 16 which results in extrapolation in simulation. In comparison to Figure 17, the difference for parameterization with CRU800-data is larger than with FB2501-data. Similarly, the smallest difference occurs when parameterizing with more appropriate data from CIB.

In conclusion, ignoring the different amount of data from manufacturers, for all the approaches presented, differences of less than approx. 3% have been presented. This verifies that `BoilerModular` is able to scale according to $\dot{Q}_b^{des}$ and to represent off-design operation compared to common modelling approaches. In addition, with only three parameters, the model is user-friendly compared to finding and evaluating efficiency data for parameterization. Furthermore, as illustrated in Figure 18, `BoilerModular` is capable of representing condensation effects with minimal parameterization effort, eliminating the need for condensation-specific parameters. Compared to `BoilerNoControl` from *AixLib* (Maier et al. 2023), `BoilerModular` is based on a physical description of off-design operation.

5. Discussion

The objective of this work is to present a user-friendly and scalable dynamic boiler model that represent natural gas

boiler operation in general. For this reason, two independent models were presented:

- The SPM creates a efficiency chart which claims to be representative describing boiler efficiencies for a wide operating range in respect to manufacturer efficiency data
- Using the aforementioned chart, the dynamic and user-friendly model `BoilerModular` is capable to simulate complex boiler operation.

Consequently, `BoilerModular` agrees with the goal by Gopisetty, Treffinger, and Xu (2014) of a simple boiler model, as it is designed by parameterization with three parameters $\dot{Q}_{\mathrm{b}}^{\mathrm{des}}$, $T_{\mathrm{return}}^{\mathrm{des}}$, and $T_{\mathrm{supply}}^{\mathrm{des}}$ resulting in a user-friendly model. In addition, condensing operation is respected without additional parameterization effort for the user. In contrast to the other stationary efficiency estimation models presented in Maier et al. (2023) and Wetter et al. (2014), a key advantage of combining the SPM with `BoilerModular` is that no manual selection of appropriate efficiency data for operating and design conditions is required. Furthermore, due to the adjustable size and step size of each dimension in the resulting efficiency chart, interpolation and extrapolation errors are negligible. Nevertheless, the simulation comparison has shown that the model's influence remains below 3%, while the operation is still considered physically plausible.

To describe boiler operation in general, the SPM introduces several assumptions regarding parameter data and modelling approaches in order to design an efficiency chart that represents a selection of manufacturer efficiency data. In the SPM, scalability was addressed by representing proportional behaviour as a function of the design heat power. As a result, boiler size has a negligible impact on boiler efficiency. However, this was only demonstrated for a uniform λ and similar exhaust gas temperatures. Moreover, part-load operation and condensation effects were not considered in the calibration. Especially for a different λ, other exhaust temperatures and condensation effects occur, which can result in a non-negligible impact on the efficiency.

For the SPM-validation, field-monitoring data was used alongside two detailed efficiency data-sets derived from manufacturer data sheets. The SPM demonstrated good agreement across all examined operating points resulting in small errors. Beyond the overall simplification, the main sources of error are likely:

- The SPM does not account for individual hardware characteristics due to regression (see Figure 5).
- The SPM assumes the thermodynamic properties of methane, leading to discrepancies when compared to manufacturer data, which is typically based on natural gas.
- The modelling of the condensation process is simplified.
- Equation (18) requires $T''_{\mathrm{ex}} \geq \bar{T}_{\mathrm{ln,W}}$, which imposes a lower bound on T''_{ex} and consequently limits η_{b}.
- A constant kA_{hex} is assumed under part-load conditions. While varying flow rates do affect heat transfer, this simplification is supported by the findings of Wang et al. (2023), who demonstrated that the total heat transfer coefficient during condensation can be up to seven times greater than the purely convective component. This indicates that convection does not constitute the dominant mechanism in such regimes. As shown in the validation, the largest deviations occur at high temperature levels under part-load conditions, where no condensation takes place. Consequently, a possible explanation is the increasing importance of convective heat transfer in the absence of condensation and film formation.

Consequently, the applicability of `BoilerModular` is constrained by the validity range of the parameters and assumptions within the SPM. However, as demonstrated by the validation, the model is capable of describing a wide operating range. For simulation purposes outside the presented operating range, the assumptions and parameters of the SPM must be re-evaluated.

However, the validation is restricted to heat power classes ranging from approximately 80 to 1870 kW. Consequently, validation for typical units around 20 kW, which are commonly used in flats and single-family houses, remains unaddressed due to the lack of available data.

Finally, as described in Figure 10, the values $\exp(-\alpha)$ are generally quite small and can be neglected. Based on validation and model comparison, this simplification is justified, allowing Equation (18) to be expressed in a simplified form, leading to Equation (32).

$$T''_{\mathrm{ex}} \approx \bar{T}_{\mathrm{ln,w}} \tag{32}$$

6. Conclusion

This paper introduces an approach for modelling a user-friendly dynamic boiler model designated as `Boiler Modular` that can support simulation based energy planning. It is part of the Modelica library *AixLib* (Maier et al. 2023). `BoilerModular` is parameterized by only three parameters: $\dot{Q}_{\mathrm{b}}^{\mathrm{des}}$, $T_{\mathrm{return}}^{\mathrm{des}}$, and $T_{\mathrm{supply}}^{\mathrm{des}}$. In addition, it presents a modular architecture and relies on detailed quasi-static efficiency charts. Since such charts

are often difficult to obtain, a SPM for boilers was introduced to generate efficiency charts from limited calibration data including condensing effects. Using a representative dataset of a single operating point derived from publicly available manufacturer sources, a calibration was performed to produce a representative efficiency chart. `BoilerModular` makes use of this representative efficiency chart. Both models, the SPM and `BoilerModular`, are independent of each other and can be applied to other use cases, either as templates for generating characteristic charts or for performing dynamic simulations using charts from other sources than the SPM.

In the SPM, a combination of physical equations, assumptions, and regressions takes place. This model characterizes the boiler using the adiabatic efficiency and is employed for a multitude of operating points in order to generate a characteristic chart. The chart is contingent upon the four operating conditions T_{return},T_{supply},y_{w}, and $y_{\Delta\text{T}}$. In `BoilerModular`, the chart represents the core of the quasi-static submodel.

A validation of the quasi-static SPM was carried out using field data and detailed efficiency charts taken from publicly available manufacturer data. Both validations demonstrate that the model can accurately represent the effects of fuel control and varying supply and return temperatures on boiler efficiency. The discussion addresses errors resulting from simplifications and assumptions made during the modelling process.

Future work can focus on test bench validation, a comparison with other dynamic models and various dynamic simulation investigations of energy systems. Additionally, dynamic investigations on heat transfer in different boiler units must be conducted to determine whether heat transfer can be treated independently of boiler size not only under static conditions but also under dynamic conditions.

Disclosure statement

No potential conflict of interest was reported by the author(s).

Funding

This work was supported by the BMWK (German Federal Ministry for Economic Affairs and Climate Action) under Grant [03EWB003B].

Nomenclature

Acronyms

BES	building energy system
HVAC	heating, ventilation and air conditioning
SDF	scientific data format
SPM	simplified physical model

Subscripts

ΔT	temperature difference
amb	ambient
b	boiler
cond	condensation
ex	exhaust
hex	heat exchanger
ln	natural logarithm
stby	standby
v	vapour
w	water

Superscripts

ad	adiabatic
des	design
dry	dry

Symbols

α	exponent -
$\bar{T}$	mean temperature K
Δh_{vap}	specific evapoartion enthalpy J kg^{-1}
ΔT	temperature difference K
$\dot{H}$	enthalpy flow W
$LMTD$	Logarithmic mean temperature difference K
$\dot{m}$	mass flow kg s^{-1}
$\dot{Q}$	heat flow W
η	efficiency -
λ	combustion-air ratio -
ϑ	temperature °C
A	surface m^2
c_{p}	specific heat capacity J/(kgK)
d	diameter m
HHV	higher heating value J kg^{-1}
k	heat transfer coefficient W/(Km^2)
L	air requirement -
l	length m
LHV	lower heating value J kg^{-1}
n	quantity mol
T	temperature K
w	relative mass flow -
x	absolute humidity kg kg^{-1}
y	relative power -
z	relative length -

Declaration of AI

ChatGPT 4o was used to improve the language and as coding assistance.

Data availability statement

The data that supporting the findings of this study, and which are not referenced, are available on request from the corresponding author, MZ.

References

Afram, A., and F. Janabi-Sharifi. 2014. "Review of Modeling Methods for HVAC Systems." *Applied Thermal Engineering* 67 (1-2): 507–519. https://doi.org/10.1016/j.applthermaleng.2014.03.055.

Andrew Bollinger, L., J. Marquant, and M. Sulzer. 2019. "Optimization-Based Planning of Local Energy Systems-Bridging the Research-Practice Gap." *IOP Conference Series: Earth and Environmental Science* 323 (1) :012077 https://doi.org/10.1088/1755-1315/323/1/012077.

Attia, S., J. L. Hensen, L. Beltrán, and A. De Herde. 2012. "Selection Criteria for Building Performance Simulation Tools: Contrasting Architects' and Engineers' Needs." *Journal of Building Performance Simulation* 5 (3): 155–169. https://doi.org/10.1080/19401493.2010.549573.

Becker, S., A. Exner, J. Hagen, and R. Krüger. 2022. DENA-GEBÄUDEREPORT 2023. Zahlen, Daten, Fakten Zum Klimaschutz Im Gebäudebestand., Deutsche Energie-Agentur.

Blervaque, H., P. Stabat, S. Filfli, M. Schumann, and D. Marchio. 2015. "Variable-Speed Air-to-Air Heat Pump Modelling Approaches for Building Energy Simulation and Comparison with Experimental Data." *Journal of Building Performance Simulation* 9 (2): 210–225. https://doi.org/10.1080/19401493.2015.1030862.

Bloess, A., W.-P. Schill, and A. Zerrahn. 2018. "Power-to-Heat for Renewable Energy Integration: A Review of Technologies, Modeling Approaches, and Flexibility Potentials." *Applied Energy* 212: 1611–1626. https://doi.org/10.1016/j.apenergy.2017.12.073.

Brooks, D. G., S. S. Carroll, and W. A. Verdini. 1988. "Characterizing the Domain of a Regression Model." *The American Statistician* 42 (3): 187–190. https://doi.org/10.1080/00031305.1988.10475559.

Bundesverband Wärmepumpe e.V., Branchenstudie. 2023. *Marktentwicklung – Prognose Handlungsempfehlungen*, Tech. Rep. Bundesverband Wärmepumpe (BWP) e.V.

Diefenbach, N., T. Loga, R. Born, M. Großklos, and C. Herbert. 2002. *Energetische Kenngrößen für Heizungsanlagen im Bestand*, Tech. Rep. Darmstadt: Institut Wohnen und Umwelt GMBH.

DIN Deutsches Institut für Normung e. V. 2018. Heating Boilers Test Code for Heating Boilers for Atomizing Oil Burners; German Version EN 304:2017.

DIN Deutsches Institut für Normung e. V. 2022. Gas-Fired Heating Boilers Part 1: General Requirements and Tests; German Version EN 15502-1:2021.

ELCO GmbH. 2013. Betriebsanleitung für die autorisierte Fachkraft R3400/R3500/R3600SB.

Glembin, J., G. Rockendorf, E. Bertram, and J. Steinweg. 2013. "A New Easy-to-Parameterize Boiler Model for Dynamic Simulations." *ASHRAE Transactions* 119:272–292.

Gopisetty, S., P. Treffinger, and Y. Xu. 2014. "Development of Simple Boiler Model Required for Energy Planning Process." In *Grand Renewable Energy 2014 Proceedings, Tokyo, Japan*.

Haller, M. Y., J. Paavilainen, L. Konersmann, R. Haberl, A. Dröscher, E. Frank, C. Bales, and W. Streicher. 2011a. "A Unified Model for the Simulation of Oil, Gas and Biomass Space Heating Boilers for Energy Estimating Purposes. Part I: Model Development." *Journal of Building Performance Simulation* 4 (1): 1–18. https://doi.org/10.1080/19401491003671944.

Haller, M. Y., J. Paavilainen, L. Konersmann, R. Haberl, A. Dröscher, E. Frank, C. Bales, and W. Streicher. 2011b. "A Unified Model for the Simulation of Oil, Gas and Biomass Space Heating Boilers for Energy Estimating Purposes. Part II: Parameterization and Comparison with Measurements." *Journal of Building Performance Simulation* 4 (1): 19–36. https://doi.org/10.1080/19401491003653629.

International Energy Agency (IEA). 2020. *Outlook for Biogas and Biomethane Prospects for Organic Growth*, Tech. Rep. International Energy Agency.

Jin, H., and J. D. Spitler. 2002. "A Parameter Estimation Based Model of Water-to-Water Heat Pumps for Use in Energy Calculation Programs." *ASHRAE Transactions* 108:3–17.

Kaletsch, A. 2020. Presse-Information Thermotechnik, Der Energiewende einen Schritt näher Bosch präsentiert Wasserstoff-Heizkessel für Wohngebäude.

Lochinvar, LLC. 2023a. Lochinvar, LLC, KNIGHT XL (KBX0400N - KBX1000N) Sales Brochure.

Lochinvar, LLC. 2023b. Lochinvar, LLC, Crest Condensing Boiler FBN0751-6001 Brochure.

Lochinvar, LLC. 2024. FTXL Commercial Boiler Sales Brochure.

Loonen, R. C. G. M., M. L. De Klijn-Chevalerias, and J. L. M. Hensen. 2019. "Opportunities and Pitfalls of Using Building Performance Simulation in Explorative R&D Contexts." *Journal of Building Performance Simulation* 12 (3): 272–288. https://doi.org/10.1080/19401493.2018.1561754.

Maier, L., D. Jansen, F. Wüllhorst, M. Kremer, A. Kümpel, T. Blacha, and D. Müller. 2023. "AixLib: An Open-Source Modelica Library for Compound Building Energy Systems from Component to District Level with Automated Quality Management." *Journal of Building Performance Simulation* 17 (2): 196–219. https://doi.org/10.1080/19401493.2023.2250521.

Max Weishaupt GmbH. 2023. Montage- und Betriebsanleitung Gas-Brennwertgerät WTC-GW 15 … 32-B.

Max Weishaupt SE. 2025. Montage- und Betriebsanleitung Gas-Brennwertkessel WTC-GB 210 … 300-A.

Mojica-Cabeza, C. D., C. E. García-Sánchez, R. Silva-Rodríguez, and L. García-Sánchez. 2021. "A Review of the Different Boiler Efficiency Calculation and Modeling Methodologies." *Informador Técnico* 86 (1): 69–93. https://doi.org/10.23850/22565035.3697.

Olympios, A. V., A. M. Pantaleo, P. Sapin, and C. N. Markides. 2020. "On the Value of Combined Heat and Power (CHP) Systems and Heat Pumps in Centralised and Distributed Heating Systems: Lessons from Multi-Fidelity Modelling Approaches." *Applied Energy* 274:115261. https://doi.org/10.1016/j.apenergy.2020.115261.

Projektträger Jülich | Forschungszentrum Jülich GmbH. 2017. Verbundvorhaben: SolaresBauen: OOM4ABDO (03SBE 0006A). https://www.enargus.de/pub/bscw.cgi/?op = enargus.eps2&q = 03SBE0006&v = 10&id = 539314.

Rätz, M., P. Henkel, P. Stoffel, R. Streblow, and D. Müller. 2024. "Identifying the Validity Domain of Machine Learning Models in Building Energy Systems." *Energy and AI* 15:100324. https://doi.org/10.1016/j.egyai.2023.100324.

Remmen, P., M. Lauster, M. Mans, M. Fuchs, T. Osterhage, and D. Müller. 2018. "TEASER: An Open Tool for Urban Energy Modelling of Building Stocks." *Journal of Building Performance Simulation*11 (1): 84–98. https://doi.org/10.1080/19401493.2017.1283539.

Schütz, T., L. Schiffer, H. Harb, M. Fuchs, and D. Müller. 2017. "Optimal Design of Energy Conversion Units and Envelopes for Residential Building Retrofits Using a Comprehensive MILP Model." *Applied Energy* 185:1–15. https://doi.org/10.1016/j.apenergy.2016.10.049.

Senkel, Anne, Carsten Bode, Jan-Peter Heckel, Oliver Schülting, Gerhard Schmitz, Christian Becker, and Alfons Kather. 2021. "Status of the TransiEnt Library: Transient Simulation of Complex Integrated Energy Systems." In *14th Modelica Conference 2021*, 187–196. Linköping: Linköping University Press. https://doi.org/10.3384/ecp21181187.

Simic, K., I. T'Jollyn, W. Faes, J. Borrajo Bastero, J. Laverge, and M. De Paepe. 2021. "Modelling of a Gas-Fired Heating Boiler Unit for Residential Buildings Based on Publicly Available Test Data." *Energy and Buildings* 253:111451. https://doi.org/10.1016/j.enbuild.2021.111451.

Sommer, T., M. Andres, and S. Diehl. 2014. "A New Implementation of the N-D Lookup Tables." In *Proceedings of the 10th International Modelica Conference, Lund, Schweden*, 885–891. Lund: Linköping University Press. https://doi.org/10.3384/ecp14096885.

SWM Infrastruktur GmbH und Co. KG. 2024. Erdgasbeschaffenheit: Jahresmittel für 2023.

Verzijlbergh, R., L. De Vries, G. Dijkema, and P. Herder. 2017. "Institutional Challenges Caused by the Integration of Renewable Energy Sources in the European Electricity Sector." *Renewable and Sustainable Energy Reviews* 75:660–667. https://doi.org/10.1016/j.rser.2016.11.039.

Viessmann Climate Solutions SE. 2022. Klimaneutral heizen mit Wasserstoff | Viessmann. https://www.viessmann.de/de/wissen/technik-und-systeme/heizen-mit-wasserstoff.html.

Viessmann Werke GmbH & Co. KG. 2017a. Datenblatt VITOPLEX 200 Niedertemperatur-Öl-/Gas-Heizkessel 700 bis 1950 kW.

Viessmann Werke GmbH & Co. KG. 2017b. Datenblatt VITOROND 200 Niedertemperatur-Öl-/Gas-Heizkessel 440 bis 1080 kW.

Viessmann Werke GmbH & Co. KG. 2017c. Datenblatt VITO CROSSAL 300 Gas-Brennwertkessel 787 bis 1400 kW.

Viessmann Werke GmbH & Co. KG. 2018a. Datenblatt VITOPLEX 200 Niedertemperatur-Öl-/Gas-Heizkessel 90 bis 560 kW.

Viessmann Werke GmbH & Co. KG. 2018b. Datenblatt VITODENS 200-W Gas-Brennwertkessel 12,0 bis 150,0 kW als Mehrkesselanlage bis 594,0 kW.

Viessmann Werke GmbH & Co. KG. 2019a. Datenblatt VITO CROSSAL 300 Gas-Brennwertkessel 87 bis 311 kW.

Viessmann Werke GmbH & Co. KG. 2019b. Datenblatt VITO CROSSAL 200 Gas-Brennwertkessel 80 bis 318 kW 240 bis 636 kW.

Viessmann Werke GmbH & Co. KG. 2019c. Datenblatt VITO CROSSAL 300 Gas-Brennwertkessel 187 bis 635 kW.

Viessmann Werke GmbH & Co. KG. 2019d. Datenblatt VITO CROSSAL 300 Gas-Brennwertkessel 400 bis 630 kW.

Viessmann Werke GmbH & Co. KG. 2019e. Datenblatt VITO CROSSAL 300 Gas-Brennwertkessel 800 bis 1000 kW.

Viessmann Werke GmbH & Co. KG. 2020. Datenblatt VITO CROSSAL 300 Gas-Brennwertkessel 2,6 bis 60 kW.

Wang, Y., J. Jiao, Y. Dai, Z. Ke, Q. Zhao, and F. Li. 2023. "Study on Heat Transfer Characteristics of Flue Gas Condensation in Narrow Gap Heat Exchangers." *Thermal Science* 27 (6): 4681–4693. https://doi.org/10.2298/TSCI221125117W.

Wetter, M., W. Zuo, T. S. Nouidui, and X. Pang. 2014. "Modelica Buildings Library." *Journal of Building Performance Simulation* 7 (4): 253–270. https://doi.org/10.1080/19401493.2013.765506.

Wirtz, M., P. Remmen, and D. Müller. 2021. "EHDO: A Free and Open-Source Webtool for Designing and Optimizing Multi-Energy Systems Based on MILP." *Computer Applications in Engineering Education* 29 (5): 983–993. https://doi.org/10.1002/cae.v29.5.

Wolf GmbH. 2009. Planungsunterlage Großkessel 450–5200 kW.

Wolf GmbH. 2015a. Montageanleitung für den Fachhandwerker Gasbrennwerttherme CGB-2 Gasbrennwert-Heiztherme CGB-2K Gasbrennwert-Kombitherme CGB2-2-14 CGB-2(K)-20 CGB-2(K)-24.

Wolf GmbH. 2015b. Montage- und Bedienungsanleitung Gas-Brennwerttherme CGB-75 Heiztherme CGB-100 Heiztherme.

Wolf GmbH. 2015c. Montageanleitung für den Fachhandwerker Gasbrennwertzentrale CGS-2 Gasbrennwertzentrale CGS-2-14/120L CGS-2-20/160L CGS-2-24/200L CGS-2-14/150R CGS-2-20/150R CGS-2-24/150R.

Wolf GmbH. 2015d. Montageanleitung für den Fachhandwerker Gasbrennwertzentrale CGW-2 Gasbrennwertzentrale wandhängend CGW-2-14/100L CGW-2-20/120L CGW-2-24/140L.

Wüllhorst, F., D. Jansen, P. Mehrfeld, and D. Müller. 2021. "A Modular Model of Reversible Heat Pumps and Chillers for System Applications." In *14th Modelica Conference 2021*, 561–568. Linköping: Linköping University Press. https://doi.org/10.3384/ecp21181561.

Wüllhorst, F., L. Maier, D. Jansen, L. Kühn, D. Hering, and D. Müller. 2023. "'BESMod – A Modelica Library Providing Building Energy System Modules." In *American Modelica Conference 2022, Dallas, October 26–28*, 9–18. Dallas, TX: Linköping University Press. https://doi.org/10.3384/ECP211869.

Wüllhorst, F., P. Mehrfeld, C. Vering, D. Hering, and D. Müller. 2022. "BESTPAR: Towards Minimal Effort in Building Energy System Simulation Parameterization." In *Proceedings of BauSim Conference 2022: 9th Conference of IBPSA-Germany and Austria, Weimar, Germany*, Vol. 9. Weimar: International Building Performance Simulation Association (IBPSA). https://doi.org/10.26868/29761662.2022.82.

Yang, H., X. Lin, H. Pan, S. Geng, Z. Chen, and Y. Liu. 2023. "Energy saving Analysis and Thermal Performance Evaluation of a Hydrogen-Enriched Natural Gas-Fired Condensing Boiler." *International Journal of Hydrogen Energy* 48 (50): 19279–19296. https://doi.org/10.1016/j.ijhydene.2023.02.027.

Zeyen, E., V. Hagenmeyer, and T. Brown. 2021. "Mitigating Heat Demand Peaks in Buildings in a Highly Renewable European Energy System." *Energy* 231:120784. https://doi.org/10.1016/j.energy.2021.120784.